

Quantum Monte Carlo calculations of the thermal conductivity of neutron star crusts

Sajad Abbar,¹ Joseph Carlson,² Huaiyu Duan,¹ and Sanjay Reddy³

¹*Department of Physics and Astronomy, University of New Mexico, Albuquerque, NM 87109*

²*Theoretical Division, Los Alamos National Laboratory, Los Alamos, NM 87545*

³*Institute for Nuclear Theory, University of Washington, Seattle, WA 98195-1550*

We use the quantum Monte Carlo (QMC) techniques to calculate the static structure function $S(q)$ of a one-component ion lattice and use it to calculate the thermal conductivity κ of high-density solid matter expected in the neutron star crust. By making detailed comparisons with the results for the thermal conductivity obtained using standard techniques based on the one-phonon approximation (OPA) valid at low temperature, and the multi-phonon harmonic approximation expected to be valid over a wide range of temperatures, we assess the temperature regime where $S(q)$ from QMC can be used directly to calculate κ . We also compare the QMC results to those obtained using classical Monte Carlo to quantitatively assess the magnitude of the quantum corrections. We find that quantum effects became relevant for the calculation of κ at temperature $T \lesssim 0.3 \Omega_P$, where Ω_P is the ion plasma frequency. At $T \simeq 0.1 \Omega_P$ the quantum effects suppress κ by about 30%. The comparison with the results of the OPA indicates that dynamical information beyond the static structure is needed when $T \lesssim 0.1 \Omega_P$. These quantitative comparisons help to establish QMC as a viable technique to calculate κ at moderate temperatures in the range $T = 0.1 - 1 \Omega_P$ of relevance to the study of accreting neutron stars. This finding is especially important because QMC is the only viable technique so far for calculating κ in multi-component systems at low-temperatures.

PACS numbers: 97.60.Jd, 26.60.Gj, 95.30.Cq

I. INTRODUCTION

Observations of transient phenomena in accreting neutron stars and magnetars [1, 2] have motivated recent attempts to model the thermal evolution of the outermost regions of the neutron star called the crust [3–6]. These studies have shown that the thermal conductivity of the crust plays a very important role in shaping temporal structure of x-ray emission from these systems. In this study we revisit the calculation of the thermal conductivity of the outer crust of the neutron star, where the typical densities are in the range of $10^8 - 10^{11} \text{ g cm}^{-3}$ and temperatures are expected to be in the range of $10^7 - 10^9$ K. Under these conditions nuclei are pressure ionized and form a solid phase at low temperature. In contrast, electrons are relativistic, weakly coupled and very degenerate. For these reasons electrons dominate the thermal conductivity of the neutron star crust.

Electron conduction in the neutron star crust is limited by electron-ion scattering. Ions in the crust have large atomic number ($25 \lesssim Z \lesssim 40$), and ionic structure and dynamics are strongly correlated by Coulomb interactions. Consequently, the amplitude for electron scattering off different ions interfere. Accounting for such interference under arbitrary ambient conditions in a multi-component plasma (MCP) is a challenging many-body problem. At low temperature and for the case when the ground state is a simple solid containing only one ion species, pioneering works by Flowers and Itoh [7] and by Yakovlev and Urpin [8] have shown that the one-phonon approximation (OPA) adequately describes the collective response of the ions which is needed to calculate the electron scattering rate. More recent studies have greatly improved the description of electron scatter-

ing in a one component plasma (OCP) by including the effects of the multi-phonon processes with the harmonic approximation [9, 10]. It is now possible to calculate the electron thermal conductivity of an OCP over the full range of temperatures of interest to neutron star astrophysics. For MCP, classical molecular dynamics has proven to be useful and is expected to provide a quantitative description of the thermal conductivity in the high temperature limit when $T \gtrsim \Omega_P$ [11]. However, neither of these methods are suitable to describe electron scattering in multi-component systems at low temperature. This observation is the primary motivation for our study here where we establish that Quantum Monte Carlo (QMC) methods, which are simply generalizable to MCP, can be used to calculate the thermal conductivity at the relatively low temperatures of interest in astrophysics.

Quantum Monte Carlo (QMC) methods have been successful in determining the ground state properties of diverse strongly correlated many-particle systems and can be adapted to study MCPs at low temperature when quantum effects become relevant. In this study, which is a first step towards developing a QMC approach to MCPs, we use the QMC method to study the ion-ion correlations in an OCP at low temperature and calculate the thermal conductivity. We also use the dynamic matrix to calculate the detailed phonon spectrum at low temperature which is in turn used to calculate κ . These calculations allow us to make quantitative comparisons between the results obtained with the Monte Carlo techniques and those obtained with various approximations used in the literature. These comparisons, allow us to reassess various theoretical approaches in some detail and provide useful new insights about the role of quantum effects, the low-energy strength of the ion response func-

tion, Bragg scattering and multi-phonon effects.

The rest of the paper is organized as follows. In Section II we review the basic properties of an OCP and define the relationship between the electron conductivity and the ion dynamical structure function $S(\omega, \mathbf{q})$. In Section III we discuss the phonon spectrum and use it to calculate $S(\omega, \mathbf{q})$ in OPA. In Section IV we describe and use both classical and quantum Monte Carlo methods to calculate the static structure function $S(q)$ and compare these results to those obtained in OPA. In Section V we calculate κ using different approaches and approximations, and we identify the temperature regimes where these approximations are valid. We also outline the strategies to extend QMC calculations to MCPs in future work. Throughout this paper we adopt the natural physical units with $\hbar = c = k_B = 1$.

II. THERMAL CONDUCTIVITY OF THE OUTER CRUST

In the simplest scenario the outer crust at given density is composed of cold catalyzed matter of a single ion species. The mass number A and charge Z of the ions are density dependent and are determined by minimizing the total energy of the system. The ground state of such matter is a strongly correlated OCP with bare nuclei immersed in a degenerate and weakly coupled electron gas. The characteristic energy of the electron is set by its Fermi momentum

$$p_F = (3\pi^2 n_e)^{1/3} \approx (25 \text{ fm})^{-1} \left(\frac{Z}{30}\right)^{1/3} \left(\frac{A}{80}\right)^{-1/3} \rho_{10}^{1/3}, \quad (1)$$

where n_e is the number density of electrons, and ρ_{10} is the mass density in units of $10^{10} \text{ g cm}^{-3}$. For the densities of interest to our study, which are typically in the range of $10^8 - 10^{11} \text{ g cm}^{-3}$, p_F is much larger than electron mass m_e , and it is a good approximation to treat electrons as ultra-relativistic. In contrast, ions are heavy and correlated. One characteristic energy is set by the ion plasma frequency

$$\Omega_P = \left(\frac{4\pi Z^2 e^2 n_I}{M}\right)^{1/2} \approx (2.9 \times 10^8 \text{ K}) \left(\frac{Z}{30}\right) \left(\frac{A}{80}\right)^{-1} \rho_{10}^{1/2}, \quad (2)$$

where $n_I = n_e/Z$ is the ion density, $M \approx Am_p$ is the mass of the ion with m_p being the proton mass, and $e^2 \approx 1/137$ is the fine structure constant in natural units.

The typical Coulomb energy is of order $Z^2 e^2/a$, where

$$a = \left(\frac{4\pi n_I}{3}\right)^{-1/3} \approx (147 \text{ fm}) \left(\frac{A}{80}\right)^{1/3} \rho_{10}^{-1/3} \quad (3)$$

is the inter-ion distance. The temperature T provides a measure of the “extractable” kinetic energy or the thermal energy of the ions. The ratio between the Coulomb energy and the thermal energy of the ions is a measure of the importance of interactions in the plasma and defines the dimensionless Coulomb parameter

$$\Gamma = \frac{Z^2 e^2}{aT}. \quad (4)$$

In a weakly coupled plasma $\Gamma \ll 1$, and Coulomb interaction can be studied within perturbation theory. Numerical simulations of the OCP have shown that ions crystallize into a solid state when $\Gamma > \Gamma_m \approx 175$ [12–14]. The melting temperature of the solid

$$T_m = \frac{Z^2 e^2}{a\Gamma_m} \approx 2.0 \Omega_P \left(\frac{Z}{30}\right) \left(\frac{A}{80}\right)^{2/3} \rho_{10}^{-1/6} \quad (5)$$

can be correspondingly defined. We note that electron screening modifies the Coulomb potential generated by the ion at large distances. The modified potential is

$$V(r) = \frac{Ze}{r} e^{-r k_{\text{TF}}}, \quad (6)$$

where

$$k_{\text{TF}} = \left(4\pi e^2 \frac{\partial n_e}{\partial \mu_e}\right)^{1/2} \xrightarrow{p_F \gg m_e} \sqrt{\frac{4e^2}{\pi}} p_F \approx (1.7a)^{-1} \left(\frac{Z}{30}\right)^{1/3} \quad (7)$$

is the Thomas-Fermi (screening) momentum. Because $k_{\text{TF}} a < 1$ for the densities of interest, screening will not greatly alter the nearest neighbor ion-ion interaction, and the Coulomb parameter of the OCP without screening continues to provide a reasonable measure of the strength of interactions and the melting temperature. In this paper we have chosen to present results at fiducial densities 10^{10} and $10^{11} \text{ g cm}^{-3}$, labelled as LD and HD, respectively. The chemical compositions in these two cases are chosen according to Page and Reddy [5] for catalyzed matter in the outer crust. We list the physical conditions of the two cases in Table I.

The dynamic structure function in the crystalline state is given by

$$S(\omega, \mathbf{q}) = \frac{1}{N} \sum_{i,j=1}^N e^{-i\mathbf{q}\cdot(\mathbf{R}_i - \mathbf{R}_j)} \times \int \frac{dt}{2\pi} e^{i\omega t} \langle e^{i\mathbf{q}\cdot\mathbf{u}_j(0)} e^{-i\mathbf{q}\cdot\mathbf{u}_i(t)} \rangle_T, \quad (8)$$

where N is the total number of ions in the crystal, \mathbf{R}_i is the equilibrium position of the ion on the i 'th site, $\mathbf{u}_i(t)$ is the displacement of this ion at time t , and $\langle \dots \rangle_T$ denotes the thermal average.

TABLE I. Key parameters for cold catalyzed matter in neutron star crust at two fiducial densities. The compositions are chosen according to Page and Reddy [5].

| Name | Lattice | ρ (g cm $^{-3}$) | Ion | a (fm) | Ω_P (10 9 K) | T_m (10 9 K) | p_F^{-1} (fm) | k_{TF}^{-1} (fm) | k_D^{-1} (fm) |
|------|---------|------------------------|-----------------------|----------|------------------------|-------------------|-----------------|--------------------|-----------------|
| LD | BCC | 10 10 | $^{84}_{34}\text{Se}$ | 149 | 0.32 | 0.75 | 24 | 249 | 62 |
| HD | BCC | 10 11 | $^{80}_{28}\text{Ni}$ | 68 | 0.87 | 1.11 | 12 | 121 | 28 |

The electron thermal conductivity κ is mainly limited by electron-ion scattering and can be written as

$$\kappa = \frac{\pi^2 T n_e}{3 \epsilon_F \nu_\kappa}, \quad (9)$$

where $\epsilon_F \approx p_F$ is the electron Fermi energy, and effective collision rate is [7]

$$\nu_\kappa = \frac{2}{3} \frac{\epsilon_F}{Z(2\pi)^3} \int_0^{2p_F} dq q^3 |v(q)|^2 S'_\kappa(q). \quad (10)$$

In the above expression

$$|v(q)|^2 = e^2 |V(q)|^2 \left(1 - \frac{q^2}{4p_F^2}\right) \quad (11)$$

is the square of the scattering matrix element for electron-ion interaction with momentum exchange \mathbf{q} , and the screened Coulomb potential generated by the ion in momentum space is

$$V(q) = \frac{4\pi Z e}{\epsilon(q) q^2}, \quad (12)$$

where

$$\epsilon(q) = 1 + \frac{k_{TF}^2}{q^2} \quad (13)$$

is the static dielectric function in the Thomas-Fermi approximation. The effects due to ion-ion correlations on electron scattering are included in Eq. (10) through

$$S'_\kappa(q) = \int_{-\infty}^{\infty} d\omega \langle S'(\omega, \mathbf{q}) \rangle_{\hat{\mathbf{q}}} w_\kappa(\omega/T, q), \quad (14)$$

where $S'(\omega, \mathbf{q})$ is the inelastic part of the dynamic structure function, $\langle \dots \rangle_{\hat{\mathbf{q}}}$ is the average over the direction of unit vector $\hat{\mathbf{q}} = \mathbf{q}/q$, and

$$w_\kappa(z = \omega/T, q) = \frac{z}{e^z - 1} \left[1 + \frac{z^2}{\pi^2} \left(\frac{3p_F^2}{q^2} - \frac{1}{2} \right) \right]. \quad (15)$$

We note that the elastic Bragg scattering does not contribute to the conductivity because it has been accounted for in the ground state which leads to the electronic band structure.

Because the response at high frequency $|\omega| \gg \Omega_P$ cannot involve collective motion of the ions, we expect that most of the strength of the dynamic response will reside at energies that are comparable to Ω_P . Therefore, when

$T \gtrsim \Omega_P$ it is a good approximation to retain only the leading terms of $w_\kappa(z, q)$ in $z = \omega/T$ in the integrand in Eq. (14), and the static approximation $S'_\kappa(q) \approx S'(q)$ is valid, where

$$S'(q) = \int_{-\infty}^{\infty} d\omega \langle S'(\omega, \mathbf{q}) \rangle_{\hat{\mathbf{q}}}, \quad (16)$$

is the inelastic part of the static structure function. At very low temperature $T \ll \Omega_P$, however, the exponential factor $1/(e^{-\omega/T} - 1)$ in $w_\kappa(z, q)$ dominates. In this limit the static approximation breaks down, and $S'_\kappa(q) \ll S'(q)$. Between these two temperature limits two competing factors in $w_\kappa(z, q)$ dominate in different ranges of q . For large-angle scattering (with large q values) the exponential factor still dominates, and $S'_\kappa(q) < S'(q)$. But for small-angle scattering (with small q values) the factor p_F^2/q^2 can dominate, and $S'_\kappa(q) > S'(q)$. We will determine these temperature limits for OCP using OPA in the next section.

III. PHONON SPECTRUM AND THE DYNAMICAL RESPONSE

At low temperature the characteristic distance scale for ion motion in lattice is

$$\lambda_I = \left(\frac{1}{2M\Omega_P} \right)^{1/2} \approx (3.2 \text{ fm}) \left(\frac{Z}{30} \right)^{-1/2} \rho_{10}^{-1/4}, \quad (17)$$

which is much shorter than the inter-ion distance a . Under these conditions the restoring force on the ion is quadratic in the displacement $\mathbf{u}_i(t)$, and the detailed phonon spectrum can be calculated by using the dynamic matrix [15, 16]

$$\mathbf{D}(\mathbf{k}) = 2 \sum_{i=1}^N \sin^2 \left(\frac{\mathbf{k} \cdot \mathbf{R}_i}{2} \right) \left[\frac{\partial^2 V(\mathbf{x})}{\partial \mathbf{x} \partial \mathbf{x}^T} \right]_{\mathbf{x}=\mathbf{R}_i}. \quad (18)$$

The phonon frequencies $\omega_s(\mathbf{k})$ ($s = 1, 2, 3$) are obtained by solving the eigenvalue equation $M\omega_s^2(\mathbf{k}) - \mathbf{D}(\mathbf{k}) = 0$, and the corresponding normalized eigenvectors $\hat{\mathbf{e}}_s(\mathbf{k})$ are the phonon polarization vectors. In the long wavelength limit, phonons have a linear dispersion relation

$$\omega_s(\mathbf{k}) = c_s(\hat{\mathbf{k}})k + \mathcal{O}(k^2), \quad (19)$$

where $c_s(\hat{\mathbf{k}})$ is the sound speed of the phonon mode in propagation direction $\hat{\mathbf{k}} = \mathbf{k}/k$. Generally speaking, polarization vectors $\hat{\mathbf{e}}_s(\hat{\mathbf{k}})$ are neither parallel nor perpendicular to $\hat{\mathbf{k}}$. However, for $ka \lesssim 1$, two of the phonon

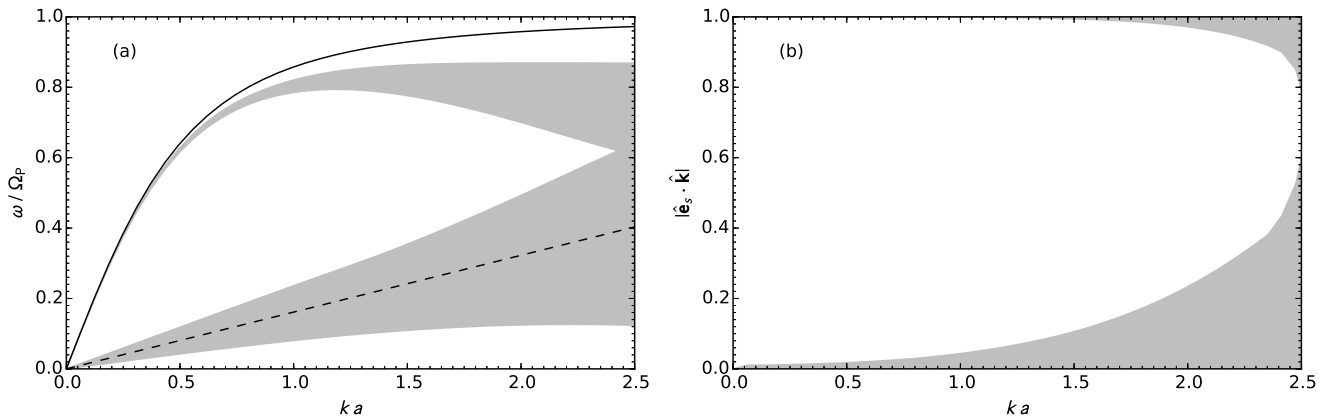


FIG. 1. The dispersion relations of the photon modes of the Coulomb lattice. Left panel: The phonon frequencies ω as functions of wave number k . The dashed and solid curves are for the transverse and longitudinal modes described by Eqs. (20) and (22), respectively. The shaded region gives the range of the eigenvalues of the dynamic matrix in Eq. (18). Right panel: The shaded region gives the range of $|\hat{\mathbf{e}}_s \cdot \hat{\mathbf{k}}|$ for the eigenvectors $\hat{\mathbf{e}}_s(\mathbf{k})$ of the dynamic matrix. The results in both panels are computed for the LD matter.

modes in a cubic lattice are approximately transverse, and the third mode is approximately longitudinal.

In Fig. 1 we show the phonon dispersion relations and polarization of a body centered cubic (BCC) lattice which are calculated from the dynamic matrix. The lower frequency modes in the left-panel of Fig. 1 correspond to the modes that are mostly transverse with $\hat{\mathbf{e}}_s \cdot \hat{\mathbf{k}} \approx 0$, and the higher frequency modes are mostly longitudinal with $|\hat{\mathbf{e}}_s \cdot \hat{\mathbf{k}}| \approx 1$.

Despite the relatively large spread of velocities associated with the transverse modes it is often useful to represent them by an “average velocity” denoted as c_t . This is typically defined by taking the limit of $k \rightarrow 0$ in which case

$$c_t = \frac{\alpha \Omega_P}{k_D} \approx 0.0031 \left(\frac{\alpha}{0.4} \right) \left(\frac{Z}{30} \right) \left(\frac{A}{80} \right)^{-2/3} \rho_{10}^{1/6}, \quad (20)$$

where $\alpha \approx 0.39$ according to Chabrier *et al.* [17], and

$$k_D = (6\pi^2 n_I)^{1/3} \approx (0.41a)^{-1} \quad (21)$$

is the Debye wave number. An approximate relation for the longitudinal mode is given by

$$\omega_l^2(k) = \frac{\Omega_P^2}{\epsilon(k)} \approx \frac{\Omega_P^2}{1 + (k_{TF}/k)^2}. \quad (22)$$

At low temperature it is useful to write the dynamic structure function as a sum of the contributions from n -phonon processes ($n = 0, 1, \dots$):

$$S(\omega, \mathbf{q}) = S^{(0)}(\omega, \mathbf{q}) + S^{(1)}(\omega, \mathbf{q}) + \dots \quad (23)$$

The elastic or Bragg scattering is the 0-phonon contribution and is given by

$$S^{(0)}(\omega, \mathbf{q}) = e^{-2W(q)} \delta(\omega) N \sum_{\mathbf{K}} \delta_{\mathbf{q}, \mathbf{K}}, \quad (24)$$

where \mathbf{K} is a reciprocal lattice vector, and

$$e^{-2W(q)} = \exp(-\langle [\mathbf{q} \cdot \mathbf{u}(0)]^2 \rangle_T) \quad (25)$$

is the Debye-Waller factor which accounts for the suppression of coherent scattering by thermal and quantum fluctuations of the ions. As mentioned earlier, the 0-phonon contribution does not affect electron scattering. At low temperature electron-ion scattering is dominated by the 1-phonon contribution

$$S^{(1)}(\omega, \mathbf{q}) = \frac{e^{-2W}}{2M} \sum_{s, \mathbf{K}} \int d^3k \frac{[\mathbf{q} \cdot \hat{\mathbf{e}}_s(\mathbf{k})]^2}{\omega_s(\mathbf{k})} \delta^3(\mathbf{K} + \mathbf{k} - \mathbf{q}) \left[\frac{\delta(\omega - \omega_s(\mathbf{k}))}{e^{\omega_s(\mathbf{k})/T} - 1} + \frac{\delta(\omega + \omega_s(\mathbf{k}))}{1 - e^{-\omega_s(\mathbf{k})/T}} \right], \quad (26)$$

where the phonon momentum \mathbf{k} is restricted to the first

Brillouin zone [7, 16]. In this case $S'_\kappa(q)$ in Eq. (10) can

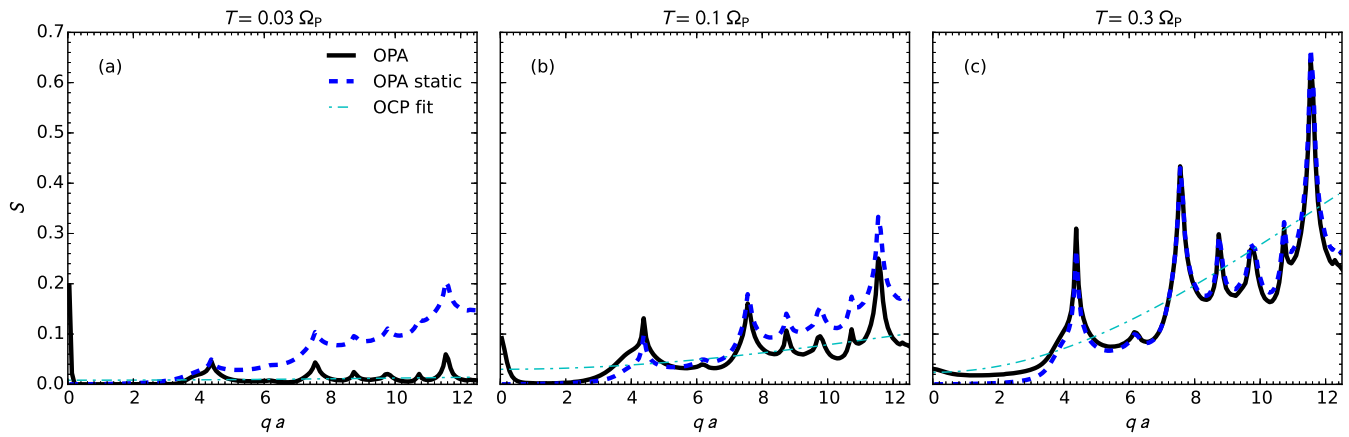


FIG. 2. (Color online) The one-phonon approximation results of $S'_\kappa(q)$ (thick solid curves) and $S'(q)$ (thick dashed curves) for the LD matter at the three temperatures as labelled. The results of $S'_\kappa(q)$ obtained using the fitting formula by Potekhin *et al.* [10], which is based on the harmonic approximation for the one-component Coulomb plasma and which includes multi-phonon contributions, are also shown (as dot-dashed curves) for comparison.

be replaced by

$$S_\kappa^{\text{OPA}}(q) = \int_{-\infty}^{\infty} d\omega \left\langle S^{(1)}(\omega, \mathbf{q}) \right\rangle_{\hat{\mathbf{q}}} w_\kappa(\omega/T, q). \quad (27)$$

Note that large-angle scattering involves a finite $|\mathbf{K}| \gg |\mathbf{k}|$ where the crystal absorbs a large component of the momentum. This is well-known as the Umklapp process in solid state physics [16]. Flowers and Itoh [7] realized that these processes dominate over normal process (with $\mathbf{K} = 0$) in the neutron star context for typical temperatures of interest because $p_F \gg k_D$. However, transitions with small \mathbf{k} and finite \mathbf{K} are suppressed due to electronic band structure effects which we shall now briefly discuss.

Although it is generally a good approximation to assume that electrons are free, on patches of the electron Fermi surface which intersect with the Brillouin zone boundaries, the effect of the periodic background ion potential is large. It distorts the Fermi surface and creates a band gap in the electron spectrum at the Fermi surface which is given by

$$\Delta\varepsilon(p_F) \simeq \frac{4e^2}{3\pi} \frac{e^{-W(p_F)} F(p_F)}{\epsilon(p_F)} p_F \quad (28)$$

where $F(p_F)$ is the charge form factor of the nucleus [18]. This gap can suppress the Umklapp processes when

$$T \lesssim T_U \simeq c_t \Delta\varepsilon(p_F), \quad (29)$$

[19–21]. From Eq. (29) we can deduce that $T_U < 10^{-2}\Omega_P$. In what follows we restrict our analysis to the regime where T is in the range $10^{-2} - 1 \Omega_P$ where the effects due to the band gap in the electron spectrum can be safely neglected [21].

To determine the temperature regimes where the static approximation $S'_\kappa(q) \approx S'(q)$ is valid, we compute the

static structure function $S'(q)$ in OPA:

$$S^{\text{OPA}}(q) = \int_{-\infty}^{\infty} d\omega \left\langle S^{(1)}(\omega, \mathbf{q}) \right\rangle_{\hat{\mathbf{q}}}. \quad (30)$$

In Fig. 2 we compare $S_\kappa^{\text{OPA}}(q)$ and $S^{\text{OPA}}(q)$ of the LD matter at three different temperatures, $T/\Omega_P = 0.03$, 0.1 and 0.3, respectively. The right panel of this figure shows that, even at $T = 0.3 \Omega_P$, $S'_\kappa(q) = S'(q)$ is already a good approximation. The left panel of Fig. 2 shows that, at low temperature $T = 0.03 \Omega_P$, the exponential factor $1/(e^{\omega/T} - 1)$ in Eq. (15) dominates, and $S'_\kappa(q) \ll S'(q)$ in most of the range of q . The middle panel of Fig. 2 with $T = 0.1 \Omega_P$ illustrates the competition between two factors in the expression of w_κ at moderate temperatures, which are discussed earlier following Eq. (16) in Section II. For large-angle scattering with $qa \gtrsim 5$ the exponential factor still dominates, and $S'_\kappa(q) < S'(q)$. For small-angle scattering with $qa \lesssim 5$, however, the factor p_F^2/q^2 dominates, and $S'_\kappa(q) > S'(q)$. We note that at low temperature $S'_\kappa(q)$ has a peak at $q \rightarrow 0$ because

$$w_\kappa(\omega/T \ll 1, qa \ll 1) \approx 1 + \frac{3}{\pi^2} \left(\frac{p_F}{T} \right)^2 \left(\frac{\omega}{q} \right)^2,$$

and the second term in this expression always dominates under the typical conditions in the neutron star crust.

For comparison we also show in Fig. 2 the results of $S'_\kappa(q)$ obtained using the fitting formula by Potekhin *et al.* [10] which is based on the harmonic approximation for the one-component Coulomb plasma and which includes multi-phonon contributions.

IV. STATIC STRUCTURE FUNCTION AND MONTE CARLO SIMULATIONS

The neutron star crust spans the regimes where purely classical simulations are sufficient and where quantum effects start to play a significant role. We can use classical and Quantum Monte Carlo simulations (CMC and QMC) to address these conditions. The QMC simulations have the classical simulations as a specific limit. Both the CMC and QMC calculations can easily address the static structure function $S(q)$. They can also be used to compute further information about the energy dependence of the response as well as other observables.

In CMC the kinetic and potential energies are independent variables. Hence the positions of the particles can be sampled independently of their momentum. We use a simple version of the Metropolis Monte Carlo method to sample the positions of the nuclei in periodic boundary conditions at fixed density and temperature. The simulations use $N \gtrsim 1000$ particles, initially at predetermined lattice sites in a periodic cubic box with length $L = (N/n_I)^{1/3}$. Proposed particle moves $\{\mathbf{x}_i\} \rightarrow \{\mathbf{x}'_i\}$ have equal transition probabilities as their reverses:

$$\mathcal{T}(\{\mathbf{x}_i\} \rightarrow \{\mathbf{x}'_i\}) = \mathcal{T}(\{\mathbf{x}'_i\} \rightarrow \{\mathbf{x}_i\}), \quad (31)$$

and they are accepted with probabilities

$$P(\{\mathbf{x}_i\} \rightarrow \{\mathbf{x}'_i\}) = \begin{cases} e^{-\Delta E/T_\sigma} & \text{if } \Delta E \geq 0, \\ 1 & \text{otherwise.} \end{cases} \quad (32)$$

For CMC $T_\sigma = T$, and the energy change is the same as the change in total potential energy:

$$\Delta E = E_{\text{pot}}(\{\mathbf{x}'_i\}) - E_{\text{pot}}(\{\mathbf{x}_i\}), \quad (33)$$

where

$$E_{\text{pot}}(\{\mathbf{x}_i\}) = \sum_{i < j} V(|\mathbf{x}_i - \mathbf{x}_j|). \quad (34)$$

In Eq. (34) the sums over i and j run over the particles in the simulation volume plus their periodic images. Typically plus or minus one image in each direction (i.e. 27 periodic boxes in total) is sufficient in these simulations because of the screening of the ion-ion potential. Standard Ewald summation is also possible but would be slower. Detailed balance ensures that the Markov chain constructed with the method described above will converge eventually to sample particle positions proportional to the partition function.

Quantum fluctuations become important when $T/\Omega_P \lesssim 1$. For such scenarios we used path integral QMC simulations (see, e.g., [22]). The single position for each particle in the classical simulation becomes a path in path integral simulations with periodic boundary conditions in imaginary time. Boson or fermion path integrals would require us to include exchanges in the imaginary time boundary conditions with the appropriate statistics, e.g. -1 for odd permutations of

fermions. Because the characteristic distance λ_I of ion motion in lattice is much shorter than the inter-ion distance a , quantum statistics (the boson or fermion nature of nuclei) is not important, and we can consider the particles as distinguishable.

In (path integral) QMC simulations the imaginary time or inverse temperature $\beta = 1/T$ is split into N_β slices. Each slice is a classical N -particle system described above but with effective temperature

$$T_\sigma = (\Delta\tau)^{-1} = \left(\frac{\beta}{N_\beta}\right)^{-1}. \quad (35)$$

For QMC each imaginary-time slice involves a high-temperature expansion of the propagator $\exp(-H\Delta\tau)$. For a large enough number of slices N_β the results are independent of the number of slices. Typically of order 10 slices are required in the present calculations.

As in CMC, the Markov chain is again constructed by moving the particles according to the acceptance probability defined in Eq. (32). For QMC the energy change includes the changes in both kinetic and potential energies:

$$\Delta E = [E_{\text{pot}}(\{\mathbf{x}'_{i,\sigma}\}) + E_{\text{kin}}(\{\mathbf{x}'_{i,\sigma}\})] - [E_{\text{pot}}(\{\mathbf{x}_{i,\sigma}\}) + E_{\text{kin}}(\{\mathbf{x}_{i,\sigma}\})], \quad (36)$$

where

$$E_{\text{kin}}(\{\mathbf{x}_{i,\sigma}\}) = \sum_{i=1}^N \sum_{\sigma=1}^{N_\beta} \frac{(\mathbf{x}_{i,\sigma+1} - \mathbf{x}_{i,\sigma})^2}{2M(\Delta\tau)^2}, \quad (37)$$

$$E_{\text{pot}}(\{\mathbf{x}_{i,\sigma}\}) = \sum_{\sigma=1}^{N_\beta} \sum_{i < j} V(|\mathbf{x}_{i,\sigma} - \mathbf{x}_{j,\sigma}|) \quad (38)$$

with $\mathbf{x}_{i,N_\beta+1} = \mathbf{x}_{i,1}$. Clearly, a CMC simulation can be considered as a special case of QMC simulation with $N_\beta = 1$.

The static structure function is then obtained from the points sampled after convergence. In Monte Carlo simulations

$$S(q) = \frac{1}{NN_\beta} \left\langle \sum_{\sigma=1}^{N_\beta} \sum_{i,j=1}^N e^{i\mathbf{q} \cdot (\mathbf{x}_{i,\sigma} - \mathbf{x}_{j,\sigma})} \right\rangle_{\hat{\mathbf{q}}, T}, \quad (39)$$

which includes both the one-phonon and multi-phonon contributions. Because of the periodic condition,

$$\mathbf{q} = \frac{2\pi}{L} (n_x \hat{\mathbf{x}} + n_y \hat{\mathbf{y}} + n_z \hat{\mathbf{z}}) \quad (40)$$

take discrete values, where $n_{x(y,z)}$ are integers. To obtain the inelastic part of the static structure function $S'(q)$ we simply remove the points that correspond to the Bragg peaks in the BCC lattice. Other detailed structures predicted by QMC and CMC, i.e. the smaller peaks and troughs away from the Bragg peaks (see Fig. 3), are finite-size artifacts whose amplitude decreases with increasing particle number in the simulation. However, the

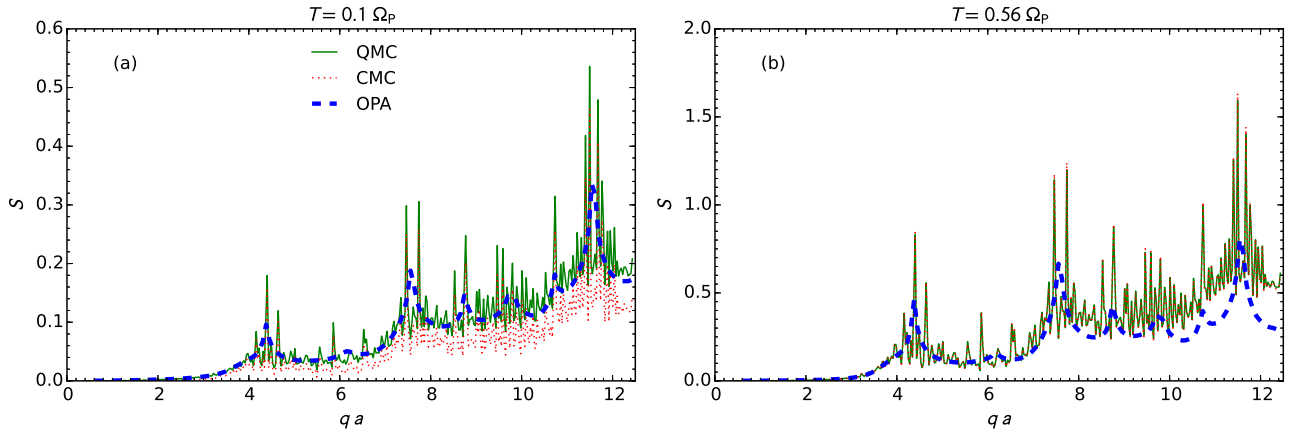


FIG. 3. (Color online) The inelastic part of static structure function $S'(q)$ of the LD matter at the two temperatures as labelled. The results are obtained using the one-phonon approximation (thick dashed curves), and quantum and classical Monte Carlo simulations (solid and dotted curves), respectively.

integrated strength over any reasonable interval in q is physically relevant and is insensitive to finite-size effects after the numerical convergence has been achieved.

At high temperature $T \gtrsim \Omega_P$ all phonon modes are excited, $S^{\text{CMC}}(q)$ and $S^{\text{QMC}}(q)$, which are $S'(q)$ obtained using CMC and QMC simulations, respectively, should agree. But at low temperature $T \ll \Omega_P$ quantum fluctuations become prominent, and $S^{\text{QMC}}(q) > S^{\text{CMC}}(q)$. In Fig. 3 we compare $S^{\text{CMC}}(q)$ and $S^{\text{QMC}}(q)$ for the LD matter at two different temperatures, $T/\Omega_P = 0.1$ and 0.56 , respectively. Indeed, $S^{\text{QMC}}(q)$ is clearly larger than $S^{\text{CMC}}(q)$ at $T = 0.1 \Omega_P$, but it is somewhat surprising that $S^{\text{CMC}}(q)$ and $S^{\text{QMC}}(q)$ agree very well even at temperature as low as $T = 0.56 \Omega_P$.

For comparison we also show $S^{\text{OPA}}(q)$ in Fig. 3. This figure shows that $S^{\text{QMC}}(q)$ and $S^{\text{OPA}}(q)$ agree with each other at low T and/or small q , although there exist rapid oscillations in Monte Carlo results because of the finite size of the system. At high T and/or large q multiphonon contributions are significant, and the one-phonon approximation breaks down.

Note that in Eq. (39) only the equal-time correlator has been evaluated. By including an offset in the imaginary times between the evaluations of positions of particles i and j ,

$$S(s\Delta\tau, q) = \frac{1}{NN_\beta} \left\langle \sum_{\sigma=1}^{N_\beta} \sum_{i,j=1}^N e^{i\mathbf{q}\cdot(\mathbf{x}_i, \sigma - \mathbf{x}_j, \sigma+s)} \right\rangle_{\hat{\mathbf{q}}, T}, \quad (41)$$

one can obtain information about the energy dependence of the response [22]. It is also possible to calculate the properties of MCP in both the classical and quantum regimes. This would require simulations significantly larger than the OCP studied here, to ensure that the periodic boundary conditions do not impact the results. Simulations of this magnitude should be readily achievable on modern parallel computers.

V. RESULTS AND DISCUSSION

We have calculated the thermal conductivity of OCP for the LD and HD ambient conditions outlined in Table I for the temperatures of interest to neutron star phenomenology. Our primary motivation to study the simple one component system was to obtain a quantitative understanding of the effects of dynamical information and quantum fluctuations at intermediate temperatures in the range $0.1 \Omega_P \lesssim T \lesssim \Omega_P$. To this end we use the various approximate methods outlined in previous sections to calculate $S'_\kappa(q)$, which is the kernel function for computing effective electron collision rate ν_κ in Eq. (10). We then calculated κ for the catalyzed neutron star matter with densities $10^{10} \text{ g cm}^{-3}$ (LD) and $10^{11} \text{ g cm}^{-3}$ (HD), respectively. The results are shown in Fig. 4 where the thermal conductivity is obtained by replacing $S'_\kappa(q)$ with $S_\kappa^{\text{OPA}}(q)$ (thick solid curves), $S^{\text{OPA}}(q)$ (thick dashed curves), $S_\kappa^{\text{OPA}}(q)$ with simple phonon dispersion relations [see Eqs. (20) and (22)] (thin solid curves), the fitting formula of $S'_\kappa(q)$ based on the harmonic approximation [10] (thin dot-dashed curves), $S^{\text{QMC}}(q)$ (filled circles) and $S^{\text{CMC}}(q)$ (filled squares), respectively.

A careful comparison of the results obtained using different approximations for the function $S'_\kappa(q)$ provides the following useful insights:

1. We find that it is adequate to set $S'_\kappa(q) = S'(q)$ in calculating κ at temperature as low as $T \approx 0.1 \Omega_P$. A comparison between the thick dashed curves obtained using $S^{\text{OPA}}(q)$ and the thick solid curves obtained using $S_\kappa^{\text{OPA}}(q)$ supports this conclusion. The validity of this approximation is expected and well known for $T \gtrsim \Omega_P$. Our results show that $S'_\kappa(q) \approx S'(q)$ even at $T = 0.3 \Omega_P$ (see Fig. 2). Our results also show that, for $0.1 \lesssim T/\Omega_P \lesssim 0.3$, this approximate method can still be used to compute κ even though $S'_\kappa(q)$ and $S'(q)$ differ. This is because there

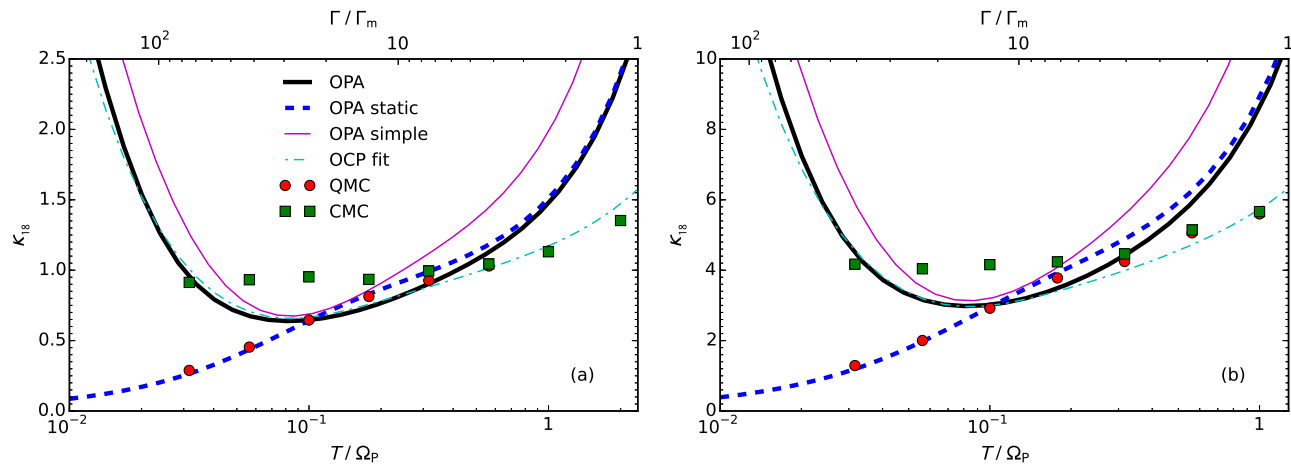


FIG. 4. (Color online) Thermal conductivity of the LD (left panel) and HD matter (right panel) in units of $10^{18} \text{ erg cm}^{-1} \text{ s}^{-1} \text{ K}^{-1}$ and as a function of temperature. The results are obtained by replacing $S'_\kappa(q)$ in Eq. (10) with $S^{\text{OPA}}_\kappa(q)$ (thick solid curves), $S^{\text{OPA}}_\kappa(q)$ (thick dashed curves), $S^{\text{OPA}}_\kappa(q)$ with approximate phonon dispersion relations [see Eqs. (20) and (22)] (thin solid curves), fitting formula of $S'_\kappa(q)$ for one-component Coulomb plasma based on the harmonic approximation [10] (thin dot-dashed curves), $S^{\text{QMC}}_\kappa(q)$ (filled circles) and $S^{\text{CMC}}_\kappa(q)$ (filled squares), respectively.

are two competing factors in $w_\kappa(\omega/T, q)$ which are discussed earlier following Eq. (30) in section II.

- Multi-phonon effects become relevant for $\Gamma/\Gamma_m \lesssim 4$ in our simulations. At higher Γ or lower temperature the one-phonon approximation is adequate for OCP but is sensitive to the phonon dispersion relation. This is evident when we compare the thick solid curves, the thin solid curves and thin dot-dashed curves, which are obtained using the exact phonon dispersion relations from the dynamical matrix, the approximate phonon dispersion relations, and the harmonic approximation method with multi-phonon contributions [10], respectively.
- The comparison between the results obtained using CMC and QMC simulations, shown by the filled squares and circles, respectively, indicates that quantum effects in thermal conductivity are significant when $T \lesssim 0.3 \Omega_P$ where classical calculations systematically underestimate $S'(q)$. At $T \approx 0.1 \Omega_P$ CMC results overestimate κ by 40 – 50%.
- The fitting formula for $S'_\kappa(q)$ based on harmonic approximation [10] (dot-dashed curves) works quite well for the one-component Coulomb lattice in the whole temperature range which we have studied. This can be seen when we compare them with the thick solid curves at $T \lesssim 0.3 \Omega_P$ and filled circles/squares at $T \gtrsim 0.3 \Omega_P$ which are obtained using the one-phonon approximation and Monte Carlo simulations, respectively. At the highest temperature where $\Gamma \approx \Gamma_m$ the results obtained using the harmonic approximation include multi-phonon excitations and agree well with the QMC results. This indicates that anharmonic effects are small

even in this regime. At the lowest temperatures, although the $S'_\kappa(q)$ obtained from the fitting formula based on the harmonic approximation differs from that obtained in the OPA (see Fig. 2), the predictions for the thermal conductivity agree well as already discussed in [10].

Some of the trends emerging from these comparisons could have been expected qualitatively. As previously alluded to, this systematic quantitative comparisons between QMC results and those obtained using the standard electron-phonon treatment provide a basis to assess the viability of using QMC calculations of $S(q)$ at low temperature for complex multi-component systems. In the standard treatment, multi-component systems are modeled as a regular lattice plus uncorrelated impurities, and electron scattering is assumed to arise due to incoherent contributions from electron-phonon and electron-impurity scattering. This treatment fails when the spatial distribution of the minority species is correlated, and QMC is a viable technique to calculate the role of these correlations in strongly coupled plasmas with $\Gamma \gg 1$ in the regime when $T < \Omega_P$.

Our results show that $S(q)$ obtained from QMC is adequate to calculate κ for $T \gtrsim 0.1 \Omega_P$, and CMC may be adequate to compute thermal conductivity of OCP at $T \gtrsim 0.3 \Omega_P$. For lower temperatures, more detailed information about the energy dependence of the response is needed and we have briefly commented on how we can access this in the discussion following Eq. (41). With a modest increase in computing resources, we have found that QMC can be used to study large multi-component plasmas, and we are currently pursuing calculations of κ for ambient conditions encountered in accreting neutron stars. These results will be reported elsewhere.

ACKNOWLEDGMENTS

This collaborative work is supported in part by the DOE Topical Collaboration on Neutrinos and Nucleosyn-

thesis in Hot and Dense Matter. H.D. thanks LANL and NMC for providing the start-up funding and the computing resources. S.R. was supported by the U.S. Department of Energy under Contract No. DE-FG02-00ER41132.

-
- [1] D. Eichler and A. F. Cheng, *Astrophys. J.* **336**, 360 (1989).
- [2] R. E. Rutledge, L. Bildsten, E. F. Brown, G. G. Pavlov, V. E. Zavlin, and G. Ushomirsky, *Astrophys. J.* **580**, 413 (2002), astro-ph/0108125.
- [3] P. S. Shternin, D. G. Yakovlev, P. Haensel, and A. Y. Potekhin, *Monthly Notices of the RAS* **382**, L43 (2007), arXiv:0708.0086.
- [4] E. F. Brown and A. Cumming, *Astrophys. J.* **698**, 1020 (2009), arXiv:0901.3115 [astro-ph.SR].
- [5] D. Page and S. Reddy, *Thermal and transport properties of the neutron star inner crust*, edited by C. Bertulani and J. Piekarewicz, *Space Science, Exploration and Policies (NOVA, 2012) Chap. 14*, arXiv:1201.5602 [nucl-th].
- [6] D. Page and S. Reddy, *Phys.Rev.Lett.* **111**, 241102 (2013).
- [7] E. Flowers and N. Itoh, *Astrophys. J.* **206**, 218 (1976).
- [8] D. G. Yakovlev and V. A. Urpin, *Soviet Astronomy* **24**, 303 (1980).
- [9] D. A. Baiko, A. D. Kaminker, A. Y. Potekhin, and D. G. Yakovlev, *Physical Review Letters* **81**, 5556 (1998), arXiv:physics/9811052.
- [10] A. Y. Potekhin, D. A. Baiko, P. Haensel, and D. G. Yakovlev, *Astronomy and Astrophysics* **346**, 345 (1999), arXiv:astro-ph/9903127.
- [11] C. J. Horowitz, O. L. Caballero, and D. K. Berry, *Phys. Rev. E* **79**, 026103 (2009), arXiv:0804.4409.
- [12] W. L. Slattery, G. D. Doolen, and H. E. DeWitt, *Phys. Rev. A* **21**, 2087 (1980).
- [13] W. L. Slattery, G. D. Doolen, and H. E. DeWitt, *Phys. Rev. A* **26**, 2255 (1982).
- [14] M. D. Jones and D. M. Ceperley, *Phys. Rev. Lett.* **76**, 4572 (1996).
- [15] W. J. Carr, *Physical Review* **122**, 1437 (1961).
- [16] N. Ashcroft and N. Mermin, *Solid State Physics* (Saunders College, Philadelphia, 1976).
- [17] G. Chabrier, N. W. Ashcroft, and H. E. Dewitt, *Nature* **360**, 48 (1992).
- [18] C. Pethick and V. Thorsson, *Phys.Rev.* **D56**, 7548 (1997), arXiv:astro-ph/9607065 [astro-ph].
- [19] J. Ziman, *Electrons and Phonons: The Theory of Transport Phenomena in Solids*, International series of monographs on physics (OUP Oxford, 1960).
- [20] M. E. Raikh and D. G. Yakovlev, *Astrophysics and Space Science* **87**, 193 (1982).
- [21] A. I. Chugunov, *Astronomy Letters* **38**, 25 (2012).
- [22] D. M. Ceperley, *Reviews of Modern Physics* **67**, 279 (1995).